Roughness-dependent tribology effects on discontinuous shear thickening

Chiao-Peng Hsu[a,b], Shivaprakash N. Ramakrishna[b], Michele Zanini[a], Nicholas D. Spencer[b], and Lucio Isa[a,1]

[a]Laboratory for Interfaces, Soft Matter and Assembly, Department of Materials, ETH Zurich, 8093 Zurich, Switzerland; and [b]Laboratory for Surface Science and Technology, Department of Materials, ETH Zurich, 8093 Zurich, Switzerland

Edited by Heinrich M. Jaeger, The University of Chicago, Chicago, IL, and accepted by Editorial Board Member Peter J. Rossky April 1, 2018 (received for review January 22, 2018)

Surface roughness affects many properties of colloids, from depletion and capillary interactions to their dispersibility and use as emulsion stabilizers. It also impacts particle–particle frictional contacts, which have recently emerged as being responsible for the discontinuous shear thickening (DST) of dense suspensions. Tribological properties of these contacts have been rarely experimentally accessed, especially for nonspherical particles. Here, we systematically tackle the effect of nanoscale surface roughness by producing a library of all-silica, raspberry-like colloids and linking their rheology to their tribology. Rougher surfaces lead to a significant anticipation of DST onset, in terms of both shear rate and solid loading. Strikingly, they also eliminate continuous thickening. DST is here due to the interlocking of asperities, which we have identified as "stick–slip" frictional contacts by measuring the sliding of the same particles via lateral force microscopy (LFM). Direct measurements of particle–particle friction therefore highlight the value of an engineering-tribology approach to tuning the thickening of suspensions.

discontinuous shear thickening | frictional contacts | roughness | nanotribology

Shear thickening (ST) is an intriguing rheological phenomenon, by which the viscosity η of a concentrated particulate suspension increases upon increasing shear rate $\dot{\gamma}$ (or shear stress σ) above a critical value (1, 2). Viscosity can either gradually increase [continuous shear thickening (CST)] or diverge at a critical shear rate [discontinuous shear thickening (DST)]. In the most extreme cases, the material can even fully solidify under flow (shear jamming) (3). DST can be either desirable, e.g., in impact-absorption applications (4), or highly detrimental, e.g., leading to clogging and pumping failures in the processing of dense slurries.

Although well characterized at the macroscale, the microscopic mechanisms governing the origins of ST are still not fully understood (5). Hydrodynamic interactions play an essential role in the viscosity increase in CST (6–10), but alone they cannot predict the viscosity divergence in DST (11–13). In contrast, dilatancy ($N_1 > 0$) is a well-known feature of dense, frictional granular materials, reflecting the formation of anisotropic force-chain networks under shear (14–16). This analogy has generated a growing consensus between theory (17), simulations (12, 18–22), and experiments (1, 13, 23–26), which have connected DST to the formation of stress-bearing structures of particles making solid–solid frictional contacts when hydrodynamic lubrication films break at high shear.

Despite this significant body of work, often the friction coefficients used in numerical simulations do not reflect realistic values and only very few studies have actually attempted to measure the frictional properties of particles experimentally, either macroscopically (22) or microscopically (23, 26), and these have been limited to smooth spheres (27). Shear-thickening systems in applications, such as cementitious slurries or the paradigmatic case of cornstarch suspensions, often comprise irregularly shaped particles. The geometry of contact is an essential component to describe frictional interactions, but, to date, only few studies have investigated the effect of particle topography, i.e., surface roughness, on ST. In general, higher roughness was shown to lead to the reduction of the onset rate and stress for DST and a sign change in N_1, from negative to positive, but no connection was made to the microscopic tribological properties of the particles (11, 13).

In this work, by experimentally studying the nanotribology of model silica colloids with tunable roughness, we demonstrate the existence of a direct link between particle topography, nanoscale friction, and macroscopic DST. Engineering of the surface design of the particles allows us to control both the critical rate and the critical solid loading for DST, driven by an interlocking mechanism that is qualitatively different from the case of smooth particles.

We fabricate our model rough colloids by electrostatic adsorption of silica nanoparticles ("berries") onto larger silica colloids ("cores"). We then grow a controlled smoothing layer via a sol-gel route, creating all-silica raspberry-like particles, as shown in Fig. 1*A* (28). Surface roughness can be tuned by independently choosing the size of the berries (12–39 nm) as well as by adjusting the thickness of the smoothing layer (10–15 nm) (Fig. 1 *B*–*G*). Surface roughness is then characterized by atomic force microscopy (AFM), and we extract a dimensionless roughness parameter h/d, calculated as the ratio between the average asperity height and the average interasperity separation, as

Significance

Shear thickening is a ubiquitous rheological phenomenon whereby dense suspensions of particles in a fluid exhibit a viscosity increase at high shear, which can turn into a viscosity divergence [discontinuous shear thickening (DST)]. Although macroscopically well characterized, the microscopic origin of DST is still debated, especially in connection to particle surface properties, e.g., roughness and friction. We elucidate here the mechanisms underpinning DST by carrying out nanotribological measurements of the interparticle contacts of model rough colloids. We demonstrate that rough particles exhibit DST over a broader range of shear rates and for volume fractions much lower than for smooth colloids, due to interlocking of surface asperities, showing that taking an engineering-tribology approach is a powerful way to tune DST.

Author contributions: N.D.S. and L.I. designed research; C.-P.H., S.N.R., M.Z., and L.I. performed research; C.-P.H., S.N.R., M.Z., N.D.S., and L.I. analyzed data; and C.-P.H., S.N.R., M.Z., N.D.S., and L.I. wrote the paper.

The authors declare no conflict of interest.

This article is a PNAS Direct Submission. H.M.J. is a guest editor invited by the Editorial Board.

[1]To whom correspondence should be addressed. Email: lucio.isa@mat.ethz.ch.

This article contains supporting information online at www.pnas.org/lookup/suppl/doi:10.1073/pnas.1801066115/-/DCSupplemental.

Published online May 1, 2018.

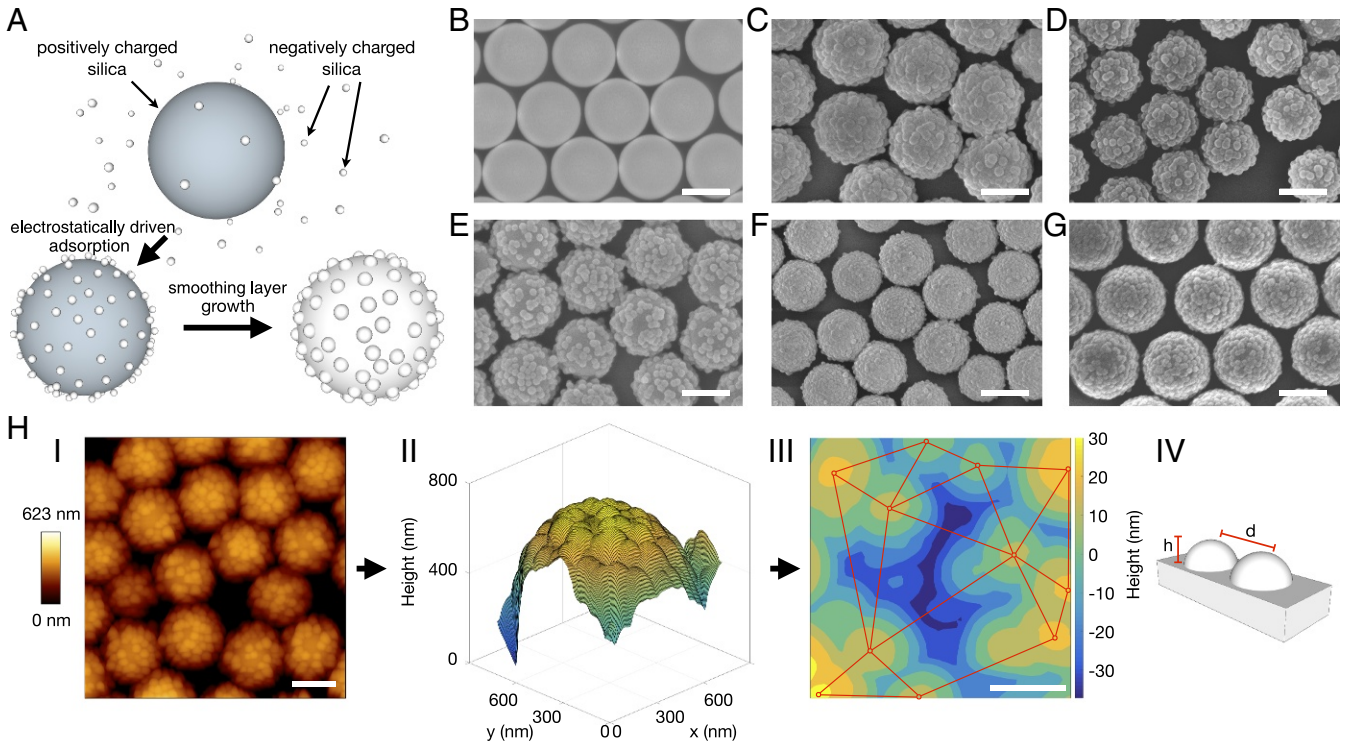

Fig. 1. Fabrication and characterization of smooth (SM) and rough (RB) particles. (*A*) Schematics of the fabrication of raspberry-like silica particles. (*B*–*G*) SEM images of (*B*) SM, (*C*) RB_0.25, (*D*) RB_0.31, (*E*) RB_0.36, (*F*) RB_0.45, and (*G*) RB_0.53. (Scale bars, 500 nm.) The numbers represent the value of h/d for each batch. (*H*, *I*–*III*) AFM image of a rough particle monolayer (*I*), 3D surface topography image of a single rough particle (*II*), and contour plot of the central region of the flattened surface of the same particle (*III*). (Scale bars: *I*, 500 nm; *II* and *III*, 100 nm.) The red circles identify the center of asperities and the red lines show the distance between asperities. (*H*, *IV*) Schematic definition of the roughness parameter h/d.

shown in Fig. 1*H*. We synthesize a library of raspberry-like silica particles with $\approx 0 < h/d < 0.53$, covering a broad roughness range from the smooth cores to the roughest raspberry. Hereon, the smooth cores are named "SM" and the raspberry-like particles "RB_h/d", where h/d is the value of the dimensionless roughness parameter for each batch. (See *SI Materials and Methods* for further details.)

We first quantify the role of surface roughness on the maximum packing fraction ϕ_m of the particles in a sedimentation/compressive rheology test. This quantity represents the limit at which the suspension can be processed, i.e., the volume fraction for which the suspension jams at vanishingly small rates. Our previous work showed that ϕ_m is directly correlated to the interparticle friction coefficient (23). As opposed to the case of non-Brownian particles, ϕ_m can slowly evolve with time due to the combined effects of thermal fluctuations and sedimentation (more details in *SI Materials and Methods* and Fig. S1). ϕ_m can be estimated by measuring the height of the sediment starting from a dilute suspension of known solid loading (Fig. 2*A*). Fig. 2*B* shows that the sediment height increases with the initial volume fraction, as expected. Rougher colloids present ϕ_m values that are clearly lower than those of smooth colloids (Fig. 2*C*). This indicates that rougher particles, i.e., with higher h/d values, jam earlier during sedimentation and, as a result, the sediment is looser. Remarkably, particles with $h/d = 0.53$ jam under centrifugation for solid loadings as low as 44.5%, indicating that roughness has a dramatic impact on DST and can be very effectively used to engineer the suspension's rheological response.

In fact, smooth colloids (SM, Fig. 2*D*) start to display CST for $\phi > 51\%$ and exhibit DST behavior only at $\phi = 58\%$, which is very close to their measured ϕ_m of 59.2%. The first normal stress difference N_1 remains negative between 48% and 58% during CST, while it switches sign at the onset of DST, which is characteristic of frictional dilatant flows. Rough colloids, on the other hand, show a qualitatively different behavior. Raspberry-like particles with $h/d = 0.53$ do not show any appreciable CST, but immediately discontinuously thicken, even for values of ϕ significantly lower than their ϕ_m (Fig. 2*E*), and the onset of DST shifts to lower $\dot{\gamma}$ with increasing ϕ. It is also worth noting that the critical rate varies over almost two decades, compared with a much narrower window for the smooth colloids. Correspondingly, the viscosity increase is always associated with a positive N_1, indicating that DST in our experiments is always associated with dilation-inducing interparticle contacts, as opposed to cases dominated by hydrodynamics, where large viscosity jumps occur for negative N_1 (29). Moreover, Fig. 2*F* shows that, at the same solid loading of $\phi = 48\%$, rough colloids with different roughnesses exhibit DST, while smooth colloids do not thicken at all. The critical DST shear rate depends on the distance from ϕ_m: The closer ϕ is to ϕ_m, the lower the observed critical shear rate. Interestingly, an analogous trend of the suspensions' nonlinear response with volume fraction and surface roughness is observed in the ball-impact tests displayed in Movies S1–S8 (*SI Materials and Methods*). Even though the deformation here is more complex (30) than in the pure shear experiments, the link between shear rheology and impact absorption has already been exploited in applications (4).

To account for these rheological observations, we turn to studying microscopic particle-to-particle contacts. These measurements are carried out by means of lateral force microscopy (LFM), where smooth and rough colloids are attached onto tipless cantilevers (Fig. S3) and scanned over planar substrates of varying roughness (roughness gradients), as shown in Fig. 3 *A* and *B* (see *SI Materials and Methods* for further details). The substrates are produced by a process analogous to the synthesis

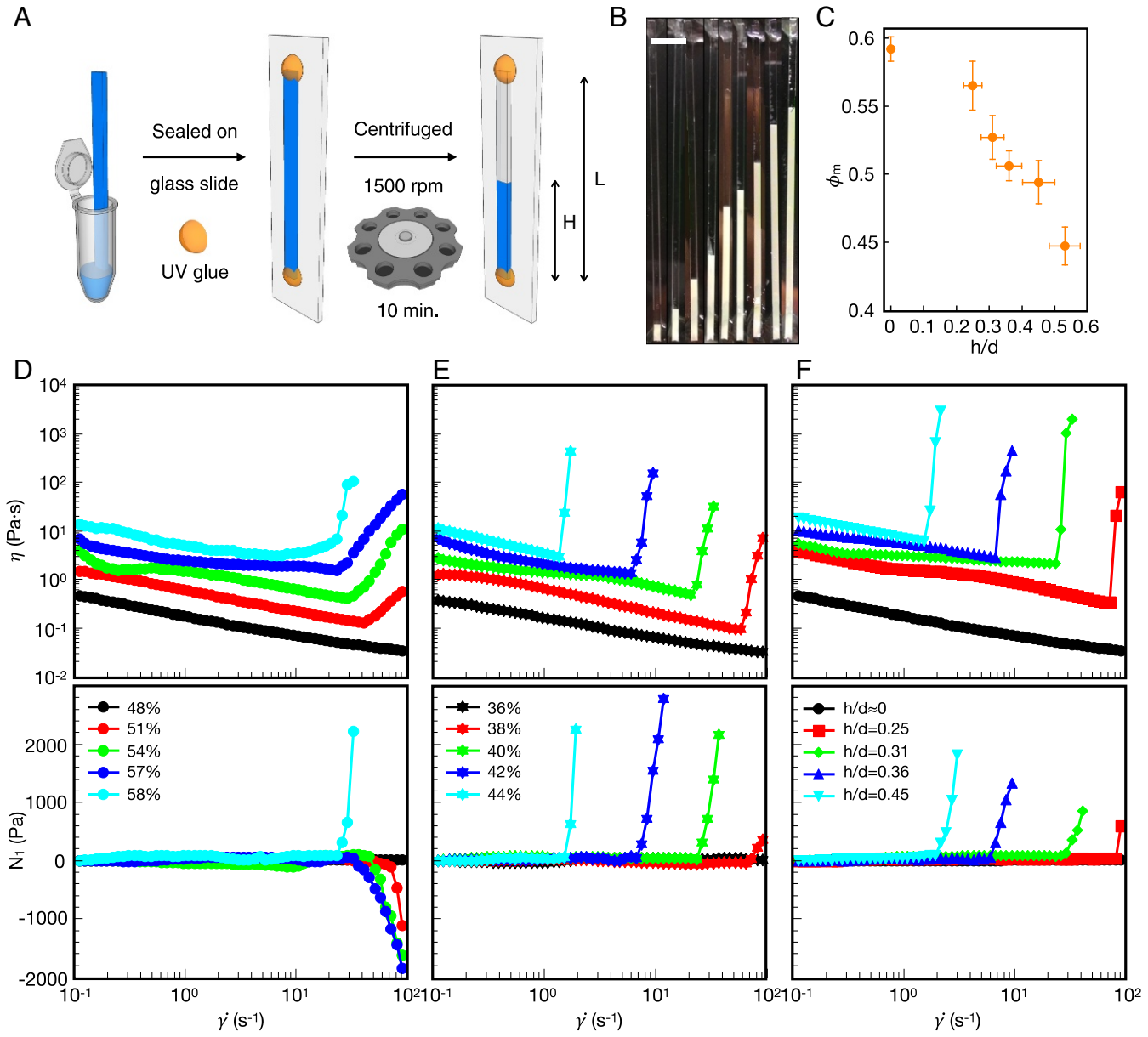

Fig. 2. Results of compressive- and shear-rheology experiments. (*A*) Schematics of the centrifugation experiments. H is the height of the sediment and L is the length of the capillary. (*B*) Images of particle suspensions (SM) after centrifugation. The initial volume fraction ϕ_i increases from 5.7% (left) to 51.6% (right). (Scale bar, 5 mm.) (*C*) ϕ_m of the colloidal suspensions with different surface roughness expressed in terms of h/d. (*D*) Flow curves (*Top*) and N_1 (*Bottom*) of smooth colloids SM (●) at different ϕ (48–58%). (*E*) Rough colloids RB_0.53 (★) at different ϕ (36–44%). (*F*) smooth colloids SM (●), rough colloids RB_0.45 (▼), rough colloids RB_0.36 (▲), rough colloids RB_0.31 (♦), and rough colloids RB_0.25 (■) at ϕ = 48%.

of the rough colloids, to provide representative, realistic countersurfaces (*SI Materials and Methods* and Fig. S2). The LFM results from sliding an RB_0.53 probe over a roughness gradient with 22-nm-high asperities are shown in Fig. 3*C*. (See Figs. S4–S7 for the friction results of all other particles.) Starting from the smooth end of the sample (Fig. 3*C*, rightmost curve, magenta), we observe a very narrow friction loop, i.e., a small difference in the lateral force signals between trace and retrace of the same scan on the substrate, indicative of a low friction coefficient. As soon as the area density of asperities increases, distinctive spikes arise in the friction-loop scans (Fig. 3*C*, cyan curve). These are typical of stick–slip frictional behavior. During scanning, when the probe meets an asperity, the lateral force increases steeply as the probe becomes locally stuck and then rapidly slides as the asperity is overcome. The frequency of the stick–slip events increases with increasing roughness (Fig. 3*C*, from right to left), which corresponds to higher dissipation during scanning and hence to an increase in the friction coefficient μ (Fig. 3*D*). We remark here that we measure "effective" friction coefficients, which already take into account the geometry of the contact, with interlocking asperities. The Amontons-type relation, $F_{friction} = \mu \cdot F_{load}$, holds very well in our experiments, as shown in Fig. 3*D*. The nature of the frictional interactions between rough surfaces also motivates our choice to describe surface roughness by the parameter h/d, since the stick–slip events are determined by the asperities' amplitude and periodicity (31), which are also the parameters we tune in the fabrication of our colloids.

Interestingly, smooth and rough probes sliding on surfaces with increasing h/d roughness give rise to different frictional

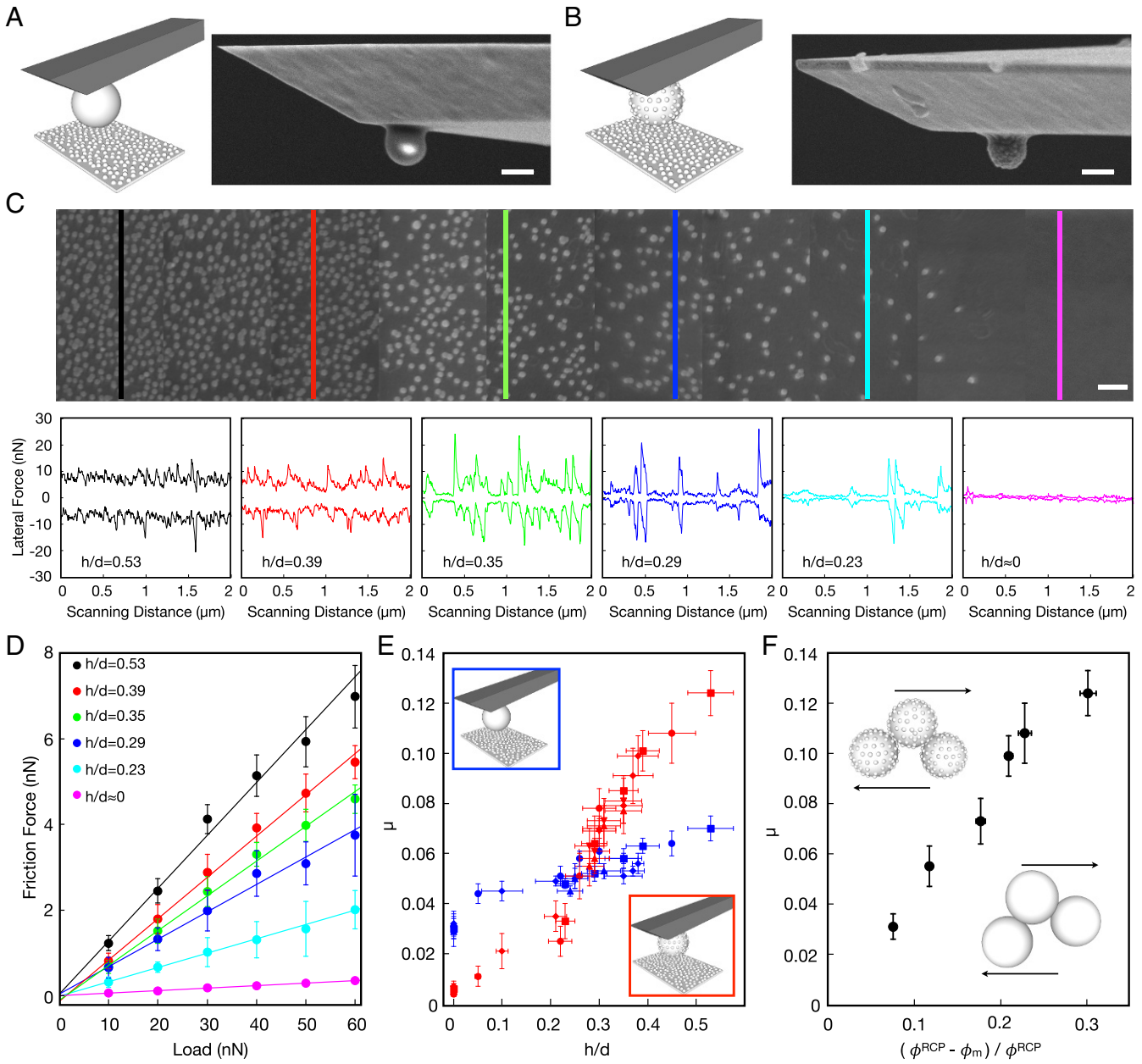

Fig. 3. Friction measurements on model rough substrates. (*A*) Schematics of a smooth probe on a rough sample and SEM image of a smooth colloidal probe. (Scale bar, 500 nm.) (*B*) Schematics of a rough probe on a rough sample and SEM image of an RB_0.53 colloidal probe. (Scale bar, 500 nm.) (*C*, *Top*) RB_0.53 probe scanning at different locations on a 22-nm rough gradient substrate. (*C*, *Bottom*) Friction loops at 60 nN applied load for various h/d roughness on the substrate (h/d = 0.53, black; h/d = 0.39, red; h/d = 0.35, green; h/d = 0.29, blue; h/d = 0.23, cyan; $h/d \approx 0$, magenta). (Scale bar, 200 nm.) (*D*) Determination of μ from the measured friction forces as a function of applied load using the relation $F_{friction} = \mu \cdot F_{load}$. (*E*) μ vs. h/d for a smooth probe (blue) and rough probes (red) on surfaces with various asperity size [12 nm (●) for RB_0.45, 22 nm (■) for RB_0.53, 39 nm (◆) for RB_0.36, and 39 nm and 12 nm (▲) for RB_0.31 and smooth and (▼) for RB_0.25]. (*E*, *Top Inset*) Schematics of a smooth probe on a rough sample. (*E*, *Bottom Inset*) Schematics of a rough probe on a rough sample. (*F*) Correlation between μ and normalized packing fraction ($\phi^{RCP} = 0.64$). (*F*, *Insets*) Schematics of smooth particles sliding (*Right*) and rough particles interlocking (*Left*) under shear.

dissipations (Fig. 3*E*). Generally, μ increases with surface roughness, but in a low-roughness regime ($h/d < 0.3$), there are fewer asperities on the substrate and μ is mainly determined by the contact area of the two sliding surfaces rather than by stick–slip events. Rough probes contact the substrate via the asperities on their surfaces, resulting in smaller contact area and hence lower μ compared with smooth probes. In particular, the values of friction coefficients measured between smooth silica probes and silica substrates are in agreement with literature values measured under similar conditions (32). Conversely, in a high-roughness regime ($h/d > 0.3$), the density of asperities on the surface increases, so that stick–slip events are the main contribution to friction forces. The asperities on raspberry-like particles interlock with the asperities on the substrates, leading to higher μ values than those measured for smooth particles. Fig. 3*E* ultimately shows that there is a direct correlation between surface roughness and friction coefficient, which uniquely depends on h/d of the two surfaces.

The unique dependence of both μ and ϕ_m on h/d makes it possible to obtain a direct relation between the first two

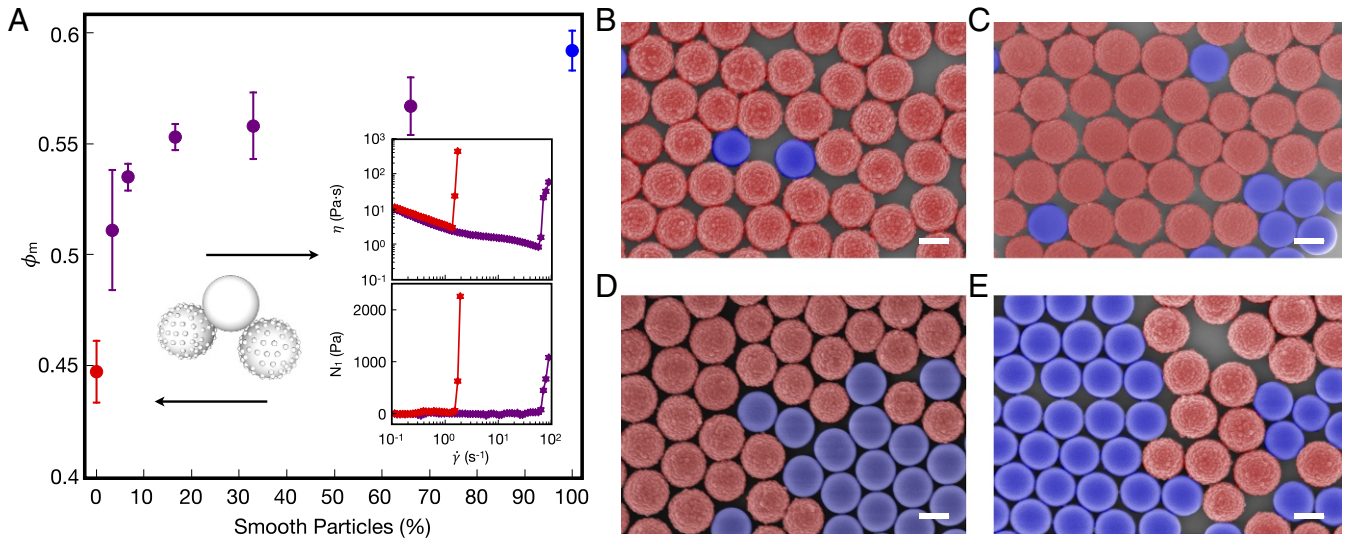

Fig. 4. Engineering the rheological response using a tribological approach. (*A*) ϕ_m of RB_0.53 (red solid circle), SM (blue solid circle), and mixed SM in RB_0.53 (purple solid circle) as a function of mixing ratio. (*A*, *Left Inset*) Schematics of a smooth particle breaking the interlocking between rough particles. (*A*, *Right Inset*) Shear viscosity (*Top*) and N_1 (*Bottom*) vs. shear rate for RB_0.53 (red solid star) and 3.3 vol% of SM in RB_0.53 (purple solid star) at ϕ = 44%. (*B*–*E*) SEM images of a suspension containing (*B*) 3.3 vol%, (*C*) 16.5 vol%, (*D*) 33.3 vol%, and (*E*) 66.6 vol% of SM (blue) in RB_0.53 (red). False colors are shown. (Scale bars, 500 nm.)

quantities, linking microscopic tribological properties with macroscopic rheological ones, as shown in Fig. 3*F*. By plotting the friction coefficients of our smooth and rough particles against surfaces with the same h/d vs. a normalized maximum packing fraction $(\phi^{RCP}-\phi_m)/\phi^{RCP}$, where $\phi^{RCP}=0.64$ is the random close packing of monodisperse frictionless spheres, we see that the higher the effective interparticle friction coefficient, the lower the maximum packing fraction at which the material can be processed before DST occurs at vanishingly small rates. Moreover, the nanotribological measurements have also shed light on the nature of the qualitative difference in the ST behavior between smooth and rough particles. For the latter, as soon as a hydrodynamic lubrication film breaks, asperities interlock, giving rise to the formation of force chains and dilatant ($N_1>0$) DST, while smooth particles experience standard sliding friction. These observations link the details of the interparticle contacts with the global rheology, in which the interlocking of many particles leads to the viscosity increase.

Finally, this correlation allows us to engineer the macroscopic rheological response, i.e., the ϕ_m of the suspension, by changing its nanoscopic tribological properties, i.e., the μ between the colloidal particles. To examine this concept, we perform the sedimentation experiments on mixed colloid suspensions obtained by introducing increasing fractions of smooth particles into suspensions of rough colloids (Fig. 4). Remarkably, by replacing as little as 3.3 vol% of the total particle number with smooth particles, ϕ_m increases by more than 6% and the onset rate for DST at $\phi=0.44$ increases by almost two decades. Increasing the percentage of smooth colloids further, ϕ_m of the mixture tends toward the ϕ_m of the suspension of smooth colloids, but the biggest effect is seen within the first 10%. This strong effect is due to the fact that smooth particles act like lubricants in the suspension by preventing strong interlocking between rough particles. The formation of a stress-bearing network is delayed or reduced, leading to denser packing before DST (note that the mixtures still exhibit DST and positive N_1).

In conclusion, our results clearly confirm that there exists a strong link between the tribology of interparticle contacts and the rheology of DST suspensions. The frictional properties greatly depend on the contact geometry, and surface roughness has emerged as an essential design parameter for the thickening response. We have, for instance, shown that one can increase the solid loading and delay undesired shear thickening by introducing a small amount of particles displaying lower friction into the system, which could be of interest for slurry processing, for example. Conversely, increasing surface roughness enables a great reduction of the volume fraction, while retaining very strong thickening but having lower viscosities in the unthickened region of the flow curve, which could be of interest in fluid materials for vibration or impact absorption. As the importance of tribology in thickening fluids is increasingly becoming more widely accepted, we expect many exciting opportunities for nanoscale surface design.

ACKNOWLEDGMENTS. We thank Jan Vermant for fruitful discussions. We thank Svetoslav Anachkov for providing the Mathematica code, Thomas Schweizer for assistance with shear-rheology measurements, Rebecca Huber for assistance with gradient-sample preparation, Christopher McLaren for help with high-speed video recording, and Andre Studart for SEM access. C.-P.H., M.Z., and L.I. acknowledge financial support from the Swiss National Science Foundation Grants PP00P2_144646/1 and PP00P2_172913/1 and the ETH Zurich Research Grant ETH-49-16-1.

1. Guy BM, Hermes M, Poon WCK (2015) Towards a unified description of the rheology of hard-particle suspensions. *Phys Rev Lett* 115:088304.
2. Brown E, et al. (2010) Generality of shear thickening in dense suspensions. *Nat Mater* 9:220–224.
3. Peters IR, Majumdar S, Jaeger HM (2016) Direct observation of dynamic shear jamming in dense suspensions. *Nature* 532:214–217.
4. Lee YS, Wetzel ED, Wagner NJ (2003) The ballistic impact characteristics of kevlarö woven fabrics impregnated with a colloidal shear thickening fluid. *J Mater Sci* 38:2825–2833.
5. Denn MM, Morris JF, Bonn D (2018) Shear thickening in concentrated suspensions of smooth spheres in Newtonian suspending fluids. *Soft Matter* 14:170–184.
6. Wagner NJ, Brady JF (2009) Shear thickening in colloidal dispersions. *Phys Today* 62:27–32.
7. Brady JF, Morris JF (1997) Microstructure of strongly sheared suspensions and its impact on rheology and diffusion. *J Fluid Mech* 348:103–139.
8. Jamali S, Boromand A, Wagner N, Maia J (2015) Microstructure and rheology of soft to rigid shear-thickening colloidal suspensions. *J Rheology* 59:1377–1395.
9. Kalman DP, Wagner NJ (2009) Microstructure of shear-thickening concentrated suspensions determined by flow-USANS. *Rheologica Acta* 48:897–908.
10. Cheng X, McCoy JH, Israelachvili JN, Cohen I (2011) Imaging the microscopic structure of shear thinning and thickening colloidal suspensions. *Science* 333:1276–1279.

11. Lootens D, van Damme H, Hemar Y, Hebraud P (2005) Dilatant flow of concentrated suspensions of rough particles. *Phys Rev Lett* 95:268302.
12. Mari R, Seto R, Morris JF, Denn MM (2014) Shear thickening, frictionless and frictional rheologies in non-Brownian suspensions. *J Rheology* 58:1693–1724.
13. Hsiao LC, et al. (2017) Rheological state diagrams for rough colloids in shear flow. *Phys Rev Lett* 119:158001.
14. Cates ME, Wittmer JP, Bouchaud JP, Claudin P (1998) Jamming, force chains, and fragile matter. *Phys Rev Lett* 81:1841–1844.
15. Heussinger C (2013) Shear thickening in granular suspensions: Interparticle friction and dynamically correlated clusters. *Phys Rev E* 88:050201.
16. Pan Z, de Cagny H, Habibi M, Bonn D (2017) Normal stresses in shear thickening granular suspensions. *Soft Matter* 13:3734–3740.
17. Wyart M, Cates ME (2014) Discontinuous shear thickening without inertia in dense non-Brownian suspensions. *Phys Rev Lett* 112:098302.
18. Seto R, Mari R, Morris JF, Denn MM (2013) Discontinuous shear thickening of frictional hard-sphere suspensions. *Phys Rev Lett* 111:218301.
19. Han E, Peters IR, Jaeger HM (2016) High-speed ultrasound imaging in dense suspensions reveals impact-activated solidification due to dynamic shear jamming. *Nat Commun* 7:12243.
20. Royer JR, Blair DL, Hudson SD (2016) Rheological signature of frictional interactions in shear thickening suspensions. *Phys Rev Lett* 116:188301.
21. Johnson DH, Vahedifard F, Jelinek B, Peters JF (2017) Micromechanical modeling of discontinuous shear thickening in granular media-fluid suspension. *J Rheology* 61:265–277.
22. Clavaud C, Berut A, Metzger B, Forterre Y (2017) Revealing the frictional transition in shear-thickening suspensions. *Proc Natl Acad Sci USA* 114:5147–5152.
23. Fernandez N, et al. (2013) Microscopic mechanism for shear thickening of non-Brownian suspensions. *Phys Rev Lett* 111:108301.
24. Lin NYC, et al. (2015) Hydrodynamic and contact contributions to continuous shear thickening in colloidal suspensions. *Phys Rev Lett* 115:228304.
25. Pan Z, de Cagny H, Weber B, Bonn D (2015) S-shaped flow curves of shear thickening suspensions: Direct observation of frictional rheology. *Phys Rev E* 92:032202.
26. Comtet J, et al. (2017) Pairwise frictional profile between particles determines discontinuous shear thickening transition in non-colloidal suspensions. *Nat Commun* 8:15633.
27. Fernandez N, Cayer-Barrioz J, Isa L, Spencer ND (2015) Direct, robust technique for the measurement of friction between microspheres. *Langmuir* 31:8809–8817.
28. Zanini M, et al. (2017) Universal emulsion stabilization from the arrested adsorption of rough particles at liquid-liquid interfaces. *Nat Commun* 8:15701.
29. Cwalina CD, Wagner NJ (2014) Material properties of the shear-thickened state in concentrated near hard-sphere colloidal dispersions. *J Rheology* 58:949–967.
30. Waitukaitis SR, Jaeger HM (2012) Impact-activated solidification of dense suspensions via dynamic jamming fronts. *Nature* 487:205–209.
31. Berman AD, Ducker WA, Israelachvili JN (1996) Origin and characterization of different stick-slip friction mechanisms. *Langmuir* 12:4559–4563.
32. Donose BC, Taran E, Vakarelski IU, Shinto H, Higashitani K (2006) Effects of cleaning procedures of silica wafers on their friction characteristics. *J Colloid Interf Sci* 299:233–237.
33. Zanini M, Hsu CP, Magrini T, Marini E, Isa L (2017) Fabrication of rough colloids by heteroaggregation. *Colloids Surf A: Physicochemical Eng Aspects* 532:116–124.
34. Bogush GH, Tracy MA, Zukoski CF (1988) Preparation of monodisperse silica particles: Control of size and mass fraction. *J Non-Crystalline Sol* 104:95–106.
35. Huwiler C, Kunzler TP, Textor M, Voros J, Spencer ND (2007) Functionalizable nanomorphology gradients via colloidal self-assembly. *Langmuir* 23:5929–5935.
36. Butt HJ, Jaschke M (1995) Calculation of thermal noise in atomic-force microscopy. *Nanotechnology* 6:1–7.
37. Varenberg M, Etsion I, Halperin G (2003) An improved wedge calibration method for lateral force in atomic force microscopy. *Rev Sci Instr* 74:3362–3367.
38. Ling X, Butt HJ, Kappl M (2007) Quantitative measurement of friction between single microspheres by friction force microscopy. *Langmuir* 23:8392–8399.